



Full length article

Confining stress path-based compressive strength model of axially compressed circular concrete-filled double-skin steel tubular short columns

Xi-Feng Yan ^a, Yan-Gang Zhao ^{a,b}, Siqi Lin ^{b,*}, Haizhong Zhang ^a

^a Department of Architecture and Building Engineering, Kanagawa University, Kanagawa 2218686, Japan

^b Key Laboratory of Urban Security and Disaster Engineering of Ministry of Education, Beijing University of Technology, Beijing 100124, China

ARTICLE INFO

Keywords:

Confining stress path (CSP)
CSP effect
Compressive strength
Concrete-filled double-skin steel tubes (CFDSTs)

ABSTRACT

Previous investigations have shown that the confining stress paths (CSPs) of confined concrete significantly affected the compressive behaviour of confined concrete in fibre-reinforced polymer (FRP) confined concrete or concrete-filled steel tube (CFST) columns. Unlike the concrete in FRP-confined concrete or CFST columns, which is only confined by external materials, e.g., FRP sheet or steel tube, the concrete in concrete-filled double-skin steel tubular (CFDST) columns is confined by both the external and internal steel tubes. Due to different confinement mechanisms, the CSPs of confined concrete in CFDST columns may be different from those in FRP-confined concrete or CFST ones, but they have not been investigated so far. In this paper, the CSPs of confined concrete in circular CFDST stub columns were experimentally investigated, and their corresponding influences on the compressive strength were also discussed. It is shown that the CSPs of confined concrete induced by the external tube are considerably influenced by column variables, whereas those generated by the internal tube found no obvious trend. Moreover, the results suggest that the compressive strength of confined concrete in specimens with a confinement coefficient η less than 2.731 is CSP-dependent, based on which, a compressive strength model of confined concrete considering the CSP effect is developed for circular CFDST columns. Based on this model, a CSP-based compressive strength model for estimating the ultimate strength of CFDST columns is proposed, and comparison with existing models against the collected test data indicates a higher accuracy of the predictions for the proposed model.

1. Introduction

Concrete-filled double-skin steel tubular (CFDST) members consist of two concentric steel tubes with different diameters, and concrete filled in the annulus between them [1,2]. Such composite cross-sections not only hold the characteristics of conventional concrete-filled steel tubes (CFSTs) counterparts [3–6], but also achieve lighter self-weight against their central cavity, higher flexural strength and better seismic resistance [7,8]. In addition, thanks to the internal tube being enclosed by external concrete, CFDST columns also possess excellent fire resistance [9]. Accordingly, they can be expected to achieve extensive applications in the sea-bed vessels, legs of offshore platforms in deep water, bridge piers, and transmission tower [7,10–13].

Various combinations of cross-sections have been declared in Ref. [3]. Of interest here are CFDST columns made of external and internal circular steel tubes, which are deemed to achieve a better confinement effect and ductility than those with other combinations [3, 14,15]. In practical engineering, two items, i.e., the compressive capacity and load–deformation relationship of a CFDST column, are deeply

concerned by engineers. Accordingly, several experimental and numerical investigations on circular CFDST columns have been performed by researchers to fully understand both items [16–28]. The results have indicated that a well established compressive strength model of confined concrete is of critical importance to accurately estimate the compressive capacity and load–deformation relationship of the CFDST columns [29].

So far, many researchers have made a lot of contributions to compressive strength models of confined concrete. Among the developed models, the models of Richard [30] and Mander [31] have been widely used in the analysis of the CFDST columns [24–27,29]. It should be noted that these models are developed based on the experimental tests of actively confined concrete, in which specimens are exposed to a constant hydrostatic lateral confining pressure during the loading process. However, in fact, the lateral stress on the confined concrete in CFDST columns varies with the axial stress during the compression process. Here, the relationship between the lateral stress and axial stress of concrete infilled during the whole loading process is defined as the confining stress path (CSP) of concrete [32–34].

* Corresponding author.

E-mail address: lsq8986@bjut.edu.cn (S. Lin).

Nomenclature

A_{is}	Cross-sectional area of inner steel tube in CFDST columns
A_{os}	Cross-sectional area of outer steel tube in CFDST columns
A_{sc}	Cross-sectional area of sandwiched concrete in CFDST columns
CI	Capacity index
D_i	Outer diameter of inner tube
D_o	Outer diameter of outer tube
E	Elastic modulus of steel tube
E_s	Tangent modulus of steel tube
f_c	Compressive strength of concrete cylinder (100 × 300 mm)
f_{ac}	Compressive strength of confined concrete under path P_a
f_{cc}	Compressive strength of confined concrete
f_{cz}	Axial concrete compressive stress
f_{sy}	Yield stress of steel
f_{syi}	Yield stress of inner tube
f_{syo}	Yield stress of outer tube
f_p	Proportional limit
G	Shear modulus
H	Gradient of equivalent plastic stress–strain curve
L	Length of column
N	Measured axial load of CFDST columns
N_m	Calculated maximum axial load of CFDST columns
$N_{u,exp}$	Measured ultimate axial load of CFDST columns
Q	Equivalent deviatoric stress variable
q	Equivalent stress variable
S_z	Axial deviatoric stress
S_θ	Circumferential deviatoric stress
SI	Dominance index
t_i	Wall thickness of inner tube
t_o	Wall thickness of outer tube
σ_e	Von Mises stress
σ_{ir}	Lateral confining stress of inner tube
σ_{or}	Lateral confining stress of outer tube
σ_{iz}	Axial stress of inner tube
$\sigma_{i\theta}$	Circumferential stress of inner tube
σ_{oz}	Axial stress of outer tube
$\sigma_{o\theta}$	Circumferential stress of outer tube
ϵ_{cz}	Axial strain of sandwiched concrete
σ_{ru}	Maximum lateral confining stress
λ	Effect index
η	Confinement coefficient
χ	Hollow ratio, given by D_i/D_o
μ	Utilization ratio of steel strength

Previous studies have checked the effects of the CSP on the compressive behaviour of confined concrete, and there are usually two different views; i.e., (1) the axial strength of confined concrete is CSP-independent [35,36]; (2) the axial strength of confined concrete is CSP-dependent [37–39]. Lately, Lim and Ozbakkaloglu [40] tested 63 actively confined and FRP-confined concrete columns under axial compression. It was shown that the axial strength of confined concrete

is CSP-dependent, and the influences of the CSPs on the behaviour of confined concrete become pronounced with raising compressive strengths of unconfined concrete. In general, the CSP effect on the behaviour of confined concrete is more significant when the confinement effect is weaker. Besides, Chin et al. [41], Xiong et al. [42], Chen et al. [43], Lai et al. [44,45], Ho et al. [46] and Lin et al. [47] analytically discussed the different behaviour between steel- or FRP-confined and actively confined concrete. On the basis of the actively confined concrete model, the analytical models considering the CSP effect for steel- or FRP-confined concrete columns were then developed. Results suggested that the CSPs are of importance to accurately capture the compressive behaviour of steel- or FRP-confined concrete columns.

It should be noted that steel- or FRP-confined concrete columns with different column parameters (i.e., geometric dimensions and material strengths) induce different CSPs, under which column behaviour is different. However, the effects of column variables on the CSPs have not been explained detailly in the above reviewed studies. To clarify the CSP, Zhao et al. [32] and Lin et al. [33,34] experimentally investigated the CSPs of confined concrete in circular CFST and FRP-confined concrete columns under different column parameters. Results suggested that the compressive strength of confined concrete in columns with a larger lateral dominant index is less CSP-dependent. Based on the experimental results, the CSP-based compressive strength models of confined concrete were suggested for the circular CFST and FRP-confined concrete columns, respectively.

However, unlike the concrete in circular FRP-confined concrete or CFST columns, which is only confined by external materials, e.g., FRP sheet or steel tube, the concrete in circular CFDST columns is confined by both the external and internal tubes [1]. Due to different confinement mechanisms, the CSPs of confined concrete in CFDST columns may be different from those in FRP-confined concrete and CFST ones, which results in the difference in the axial strength of confined concrete. This may cause some deviation in predicting the axial compression performance of CFDST columns, which includes the compressive capacity and load–deformation relationship of the CFDST columns. However, to the authors' knowledge, the CSPs of confined concrete in CFDST columns have not been investigated so far. In order to adequately understand the behaviour of confined concrete in a circular CFDST column, the CSPs of the circular CFDST columns and their corresponding effect need to be investigated.

This paper aims at experimentally investigating the CSPs of confined concrete in circular CFDST columns and discuss the corresponding CSP effect on the compressive strength of confined concrete. The remainder of this research work is outlined as: In Section 2, the details of 28 axially loaded CFDST short column specimens and the corresponding experimental tests are presented. CSP's determination and its corresponding effect are defined in detail. In Section 3, the CSPs of confined concrete in circular CFDST columns and the corresponding CSP effect on the compressive strength of confined concrete are investigated. In Section 4, a CSP-based compressive strength model for estimating the ultimate strength of CFDST columns is proposed. Finally, the conclusions are presented in Section 5.

2. Experimental tests to investigate the confining stress paths (CSPs)

2.1. Experimental program

In this section, in order to investigate the CSPs and the corresponding CSP effects on the compressive strength of confined concrete in the studied CFDST columns, an experimental program that consists of 28 specimens was performed. 24 CFDST specimens were compiled from the previous paper published by the authors [1], and 4 additional CFST specimens (a special case; the hollow ratio of CFDST column is equal to zero) were newly tested in the current paper and added as compared counterparts. All specimens can be divided into 4 groups, i.e., G1, G2,

Table 1
Details of 28 circular CFDST short column specimens.

Groups	Specimens	External steel tube			Internal steel tube			f_c (MPa)	$N_{u,exp}$ (kN)	CI	η	SI	λ	$\mu(1.045)$	$\epsilon_{cz,max}(\mu\epsilon)$
		D_o (mm)	t_o (mm)	D_o/t_o	D_i (mm)	t_i (mm)	D_i/t_i								
G1	C4-36-0-5WL-1	189.2	5.11	37.0	0.0	0.00	0.0	37.5	2374	1.21	0.53	0.18	0.57	1.052	4950
	C4-36-0-5WL-2	187.7	5.09	36.9	0.0	0.00	0.0	37.5	2390	1.23	0.53	0.17	0.60	1.050	4978
	C4-36-0.18-5WL-1	190.6	5.15	37.0	34.0	3.08	11.0	37.5	2718	1.31	0.51	0.17	0.51	1.047	5009
	C4-36-0.18-5WL-2	190.5	5.13	37.1	33.9	3.10	10.9	37.5	2724	1.32	0.51	0.16	0.43	1.046	5020
	C4-36-0.31-5WL-1	190.5	5.15	37.0	59.6	3.32	18.0	37.5	2718	1.30	0.48	0.13	0.33	1.045	4999
	C4-36-0.31-5WL-2	188.2	5.04	37.3	59.1	3.28	18.0	37.5	2482	1.22	0.47	0.14	0.35	1.045	4982
	C4-36-0.53-5WL-1	190.7	5.11	37.3	101.6	4.03	25.2	37.5	2626	1.24	0.38	0.09	0.25	1.022	4890
	C4-36-0.53-5WL-2	189.2	5.08	37.2	101.2	4.05	25.0	37.5	2462	1.18	0.37	0.09	0.26	1.032	4888
G2	C9-36-0-5WL-1	189.6	5.09	37.2	0.0	0.00	0.0	37.5	3168	1.37	0.70	0.23	0.65	1.068	5200
	C9-36-0-5WL-2	190.1	5.07	37.5	0.0	0.00	0.0	37.5	3138	1.35	0.70	0.22	0.60	1.061	5190
	C9-36-0.18-5WL-1	188.9	5.09	37.1	33.7	3.09	10.9	37.5	3182	1.34	0.68	0.21	0.47	1.055	5315
	C9-36-0.18-5WL-2	188.9	5.12	36.9	33.5	3.06	10.9	37.5	3232	1.36	0.69	0.2	0.45	1.058	5299
	C9-36-0.31-5WL-1	191.0	5.15	37.1	59.4	3.31	17.9	37.5	3286	1.34	0.64	0.18	0.36	1.047	5120
	C9-36-0.31-5WL-2	190.1	5.11	37.2	59.1	3.29	18.0	37.5	3242	1.34	0.64	0.16	0.34	1.046	5100
	C9-36-0.53-5WL-1	190.7	5.15	37.0	101.1	4.10	24.7	37.5	3082	1.24	0.51	0.12	0.28	1.022	4999
	C9-36-0.53-5WL-2	190.7	5.09	37.5	100.9	4.07	24.8	37.5	3192	1.29	0.50	0.09	0.27	1.028	5050
G3	C4-24-0.31-5WL-1	190.4	5.15	37.0	59.9	3.33	18.0	29.0	2460	1.30	0.62	0.23	0.52	1.044	4870
	C4-24-0.31-5WL-2	190.0	5.11	37.2	59.1	3.31	17.9	29.0	2494	1.32	0.61	0.19	0.51	1.045	4900
	C4-36-0.31-5WL-1	189.1	5.10	37.1	59.4	3.35	17.7	37.5	2623	1.27	0.48	0.17	0.41	1.042	4955
	C4-36-0.31-5WL-2	190.1	5.07	37.5	59.7	3.35	17.8	37.5	2588	1.25	0.47	0.13	0.43	1.045	4980
	C4-48-0.31-5WL-1	189.9	5.12	37.1	58.9	3.31	17.8	51.0	2950	1.24	0.35	0.09	0.33	1.035	4858
	C4-48-0.31-5WL-2	188.6	5.08	37.1	58.9	3.33	17.7	51.0	3026	1.29	0.35	0.08	0.35	1.034	4850
G4	C4-36-0.31-4WL-1	190.3	4.26	44.7	59.4	3.36	17.7	37.5	2376	1.24	0.38	0.13	0.45	1.045	4755
	C4-36-0.31-4WL-2	190.1	4.21	45.2	59.3	3.30	18.0	37.5	2406	1.27	0.38	0.14	0.52	1.043	4770
	C4-36-0.31-5WL-1	189.7	5.12	37.1	59.5	3.32	17.9	37.5	2611	1.26	0.48	0.17	0.47	1.048	4905
	C4-36-0.31-5WL-2	188.8	5.08	37.2	59.5	3.31	18.0	37.5	2579	1.26	0.47	0.15	0.56	1.049	4920
	C4-36-0.31-6WL-1	189.1	6.77	27.9	59.7	3.34	17.9	37.5	2894	1.27	0.61	0.16	0.64	1.052	5290
	C4-36-0.31-6WL-2	188.6	6.73	28.0	59.8	3.33	18.0	37.5	2928	1.30	0.60	0.19	0.63	1.059	5310

G3 and G4, and their details are listed in Table 1. Material properties of external and internal tubes used in the specimens are listed in Table 2. G1 and G2 were employed to check the effects of hollow ratio (χ) and outer tube yield stress (f_{syo}), whereas G3 and G4 were utilized to check the effects of concrete strength (f_c) and outer tube diameter-to-wall thickness ratio (D_o/t_o), respectively. For definition of 'label', take C4-24-0.31-5WL-1 as an example; 'C4' indicates that the column is made by the circular hollow tube with steel type STK400 (C9; steel type STK490) [1]; '24' represents the nominal concrete cylinder strength (150×300 mm), 24 MPa; '0.31' symbolizes the column with a hollow ratio of 0.31, calculated by D_i/D_o ; '5WL' indicates that the nominal outer tube wall thickness is 5 mm and the whole section of column (both concrete and steel tubes) suffers the axial loading; '1' stands for the first test objective of the identical specimens in each subset. All specimens are 570 mm in height. A schematic of the test device is presented in Fig. 1, and the detailed description can be found in Ref. [1]. It should be noted that the strain gauges attached to the middle section of column will be used to obtain the CSP.

2.2. Experimental results

After testing, the final deformed shapes of all specimens (take one of the two identical specimens as example) are shown in Fig. 2. In Fig. 2, as the original chalk marks fell off, the yellow marks were added to the pictures again. In addition, arrows and labels were attached to highlight the failure modes in Fig. 2. From this figure, it can be observed that the outward local buckling occurred at the mid-height and two ends of the external tubes. As the authors reported in Ref. [1], the inward local buckling generally occurred at the mid-height of the internal tubes. Note that the axial loads of all specimens have been normalized with regard to the whole cross-sectional area since the cross-sectional areas of the specimens are not identical. Subsequently, the axial stress versus axial/circumferential strain (unit: $\mu\epsilon$) curves of the external and internal tubes for G1, G2, G3 and G4 specimens are shown in Figs. 3 and 4,

respectively. For brevity's sake, Figs. 3 and 4 present only one curve from each two identical specimens.

Moreover, the strain compatibility is discussed here to identify the failure sequence of steel tubes and concrete. As recommended by Le et al. [25], external steel tube should reach its yield strength before the sandwiched concrete reaches its peak stress. Otherwise, a CFDST column cannot attain its full plastic response due to the brittle failure of sandwiched concrete after attaining the confined concrete strength. Hence, it should ensure that the yield strain ϵ_{syo} of the external steel tube is smaller than the compressive strain $\epsilon_{cz,max}$ of sandwiched concrete at its peak stress. The peak compressive strain of sandwiched concrete and the yield strain of steel tubes are given in Tables 1 and 2, respectively. From Tables 1 and 2, it can be concluded that the experimental results meet the recommendation of Le et al. [25]. In addition, Le et al. [25] also suggested that external steel tube should attain its yield strength before the internal steel tube reaches its yield stress. If this condition is reversed, the CFDST column would have a structural response without the internal steel tube. Hence, the yield stress of external steel tube should be less than that of inner steel tube. According to Tables 1 and 2, except that G2 specimens has higher yield stress of external steel tube, the yield stresses of the external and internal steel tubes in G1, G3 and G4 are very close. This may lead to the weak or no confinement effect of the internal steel tube on the sandwiched concrete, which is consistent with the findings of the CSP investigation in Section 3.

To evaluate the composite effects of the steel tubes and concrete in the studied CFDST specimens, a capacity index (CI) is defined here and expressed by:

$$CI = \frac{N_{u,exp}}{N_{u,sum}} \quad (1)$$

in which $N_{u,exp}$ denotes the measured ultimate axial load of the CFDST column, as shown in Table 1; $N_{u,sum}$ stands for the summation of the individual strengths of the external and internal tubes as well as the sandwiched concrete, i.e., $N_{u,sum} = f_{syo}A_{os} + f_cA_{sc} + f_{syt}A_{is}$.

Table 2
Material properties of external and internal steel tubes.

Type of steel	Location	Nominal sectional size (mm)	f_{sy} (MPa)	f_{su} (MPa)	E_o (GPa)	ϵ_{sy} ($\mu\epsilon$)
C4	Internal steel tube	34.0 × 3.10	348.2	436.7	200.4	2438
		60.0 × 3.35	342.1	435.9	198.3	2325
		101.6 × 4.10	345.8	431.6	199.7	2532
	External steel tube	190.7 × 4.30	336.8	410.6	201.3	2373
		190.7 × 5.30	346.9	429.8	202.1	2416
		190.7 × 6.80	327.3	406.3	200.4	2633
C9	External steel tube	190.7 × 5.30	464.0	515.1	199.5	2826

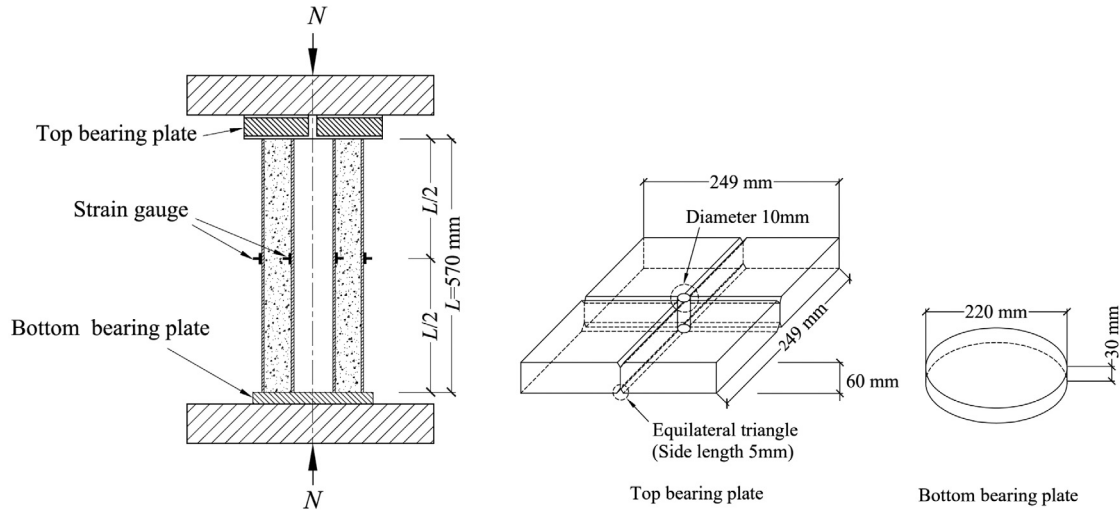


Fig. 1. Schematic of test device.

The capacity indices (*CI*s) of all the specimens calculated by Eq. (1) are listed in Table 1 and depicted in Fig. 5. From this figure, it can be found that the *CI* decreases as χ , f_c and D_o/t_o ratio increase, while it increases as f_{syo} raises. That is, the composite effects of the steel tubes and concrete infill are weakened as χ , f_c and D_o/t_o ratio increase, but they are improved as f_{syo} raises.

2.3. Determination of CSPs

As defined by the authors in Refs. [32,34], in the current paper, the typical CSP of confined concrete is defined as the relationship between the lateral confining stress (σ_r) and the ratio of axial concrete compressive stress divided by unconfined concrete strength (f_{cz}/f_c). A typical stress state diagram for circular CFDST columns is given in Fig. 6. It should be noted that, unlike the concrete in a circular FRP-confined concrete or CFST columns, which is only confined by external FRP-sheet or steel tube, the concrete in a circular CFDST column are confined by both the external and internal steel tubes. Therefore, in a CFDST column, two different CSPs may be yielded based on the confinement mechanisms of the external and internal tubes. The lateral confining stresses σ_{or} and σ_{ir} induced by the external and internal tubes and the corresponding axial concrete compressive stress f_{cz} can be determined by Eqs. (2) to (4):

$$\sigma_{or} = \frac{-2\sigma_{o\theta}t_o}{D_o - 2t_o} \quad (2)$$

$$\sigma_{ir} = \frac{2\sigma_{i\theta}t_i}{D_i} \quad (3)$$

$$f_{cz} = \frac{N - \sigma_{oz}A_{os} - \sigma_{iz}A_{is}}{A_{sc}} \quad (4)$$

where N represents the measured axial load of the column; D_o and D_i symbolize the outer diameters of the external and internal tubes, respectively, and the corresponding wall thicknesses are t_o and t_i , respectively; A_{os} and A_{is} represent the cross-sectional areas of the

external and internal tubes, respectively; A_{sc} stands for the cross-sectional area of the sandwiched concrete; σ_{oz} and $\sigma_{o\theta}$ denote the axial and circumferential stresses of the external tube, respectively; σ_{iz} and $\sigma_{i\theta}$ symbolize the axial and circumferential stresses of the internal tube, respectively. Through the following procedures, the axial and circumferential stresses can be computed by using the readings from the measured strains pasted on the surfaces of steel tubes.

The von Mises stress (or the equivalent stress) σ_e is introduced to identify the stress state of the steel tube:

$$\sigma_e = \sqrt{\sigma_z^2 - \sigma_z\sigma_\theta + \sigma_\theta^2} \quad (5)$$

where σ_z and σ_θ denote the axial and circumferential stresses of the steel tube, respectively.

In the elastic phase ($\sigma_e < f_y$), the stress components of the steel tube can be computed by the generalized Hooke's Law:

$$\begin{Bmatrix} d\sigma_z \\ d\sigma_\theta \end{Bmatrix} = \frac{E_s}{1 - \nu_s^2} \begin{bmatrix} 1 & \nu_s \\ \nu_s & 1 \end{bmatrix} \begin{Bmatrix} d\epsilon_z \\ d\epsilon_\theta \end{Bmatrix} \quad (6)$$

where $d\epsilon_z$ and $d\epsilon_\theta$ denote the axial and circumferential strain increments of steel tube, respectively; ν_s and E_s represent the Poisson's ratio and tangent modulus of steel tube respectively, and they can be determined by:

$$\nu_s = \begin{cases} 0.283 & \sigma_e < f_p \\ 0.217 \frac{\sigma_e - f_p}{f_{sy} - f_p} + 0.283 & f_p \leq \sigma_e \leq f_{sy} \\ 0.5 & \sigma_e > f_{sy} \end{cases} \quad (7)$$

$$E_s = \begin{cases} E & \sigma_e < f_p \\ (f_{sy} - \sigma_e) \sigma_e E & f_p \leq \sigma_e \leq f_{sy} \\ (f_{sy} - f_p) f_p & \sigma_e > f_{sy} \end{cases} \quad (8)$$

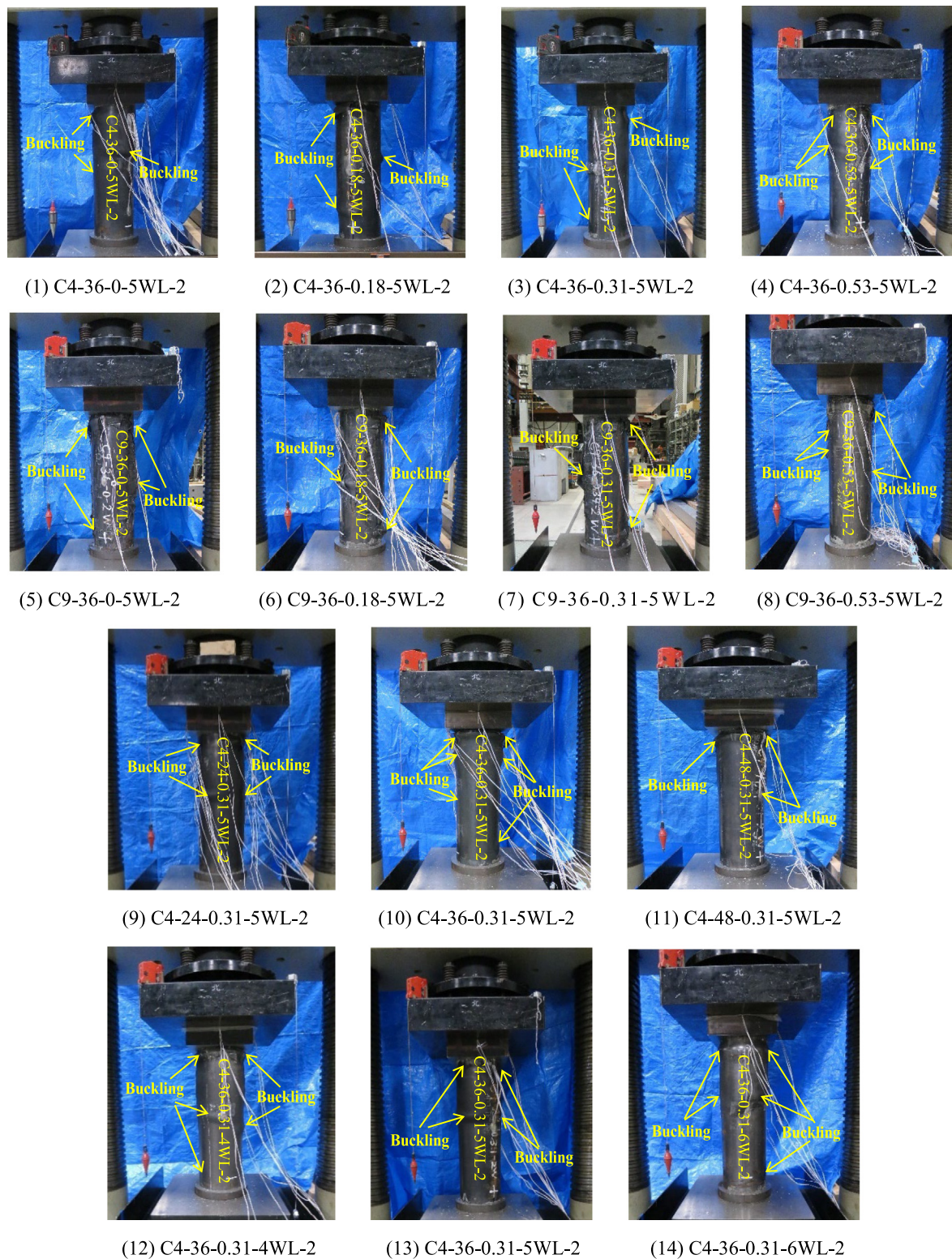


Fig. 2. Failure modes of circular CFDST specimens. (For interpretation of the references to colour in this figure legend, the reader is referred to the web version of this article.)

where E denotes the elastic modulus, f_{sy} symbolizes the steel yield stress, and f_p represents the proportional limit, herein, assumed to be $0.75 f_{sy}$.

In the plastic phase ($\sigma_e \geq f_{sy}$), the stress of the steel tube can be computed by the incremental Prandtl–Reuss equations:

$$\begin{Bmatrix} d\sigma_z \\ d\sigma_\theta \end{Bmatrix} = \frac{E_s}{Q} \begin{bmatrix} S_\theta^2 + 2q & -S_z S_\theta + 2v_s q \\ -S_z S_\theta + 2v_s q & S_z^2 + 2q \end{bmatrix} \begin{Bmatrix} d\epsilon_z \\ d\epsilon_\theta \end{Bmatrix} \quad (9)$$

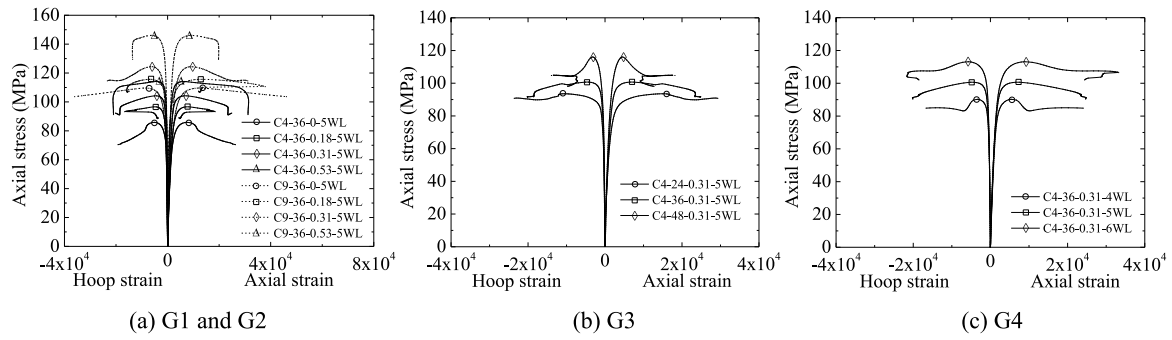


Fig. 3. Axial stress vs. strain curves of outer steel tubes.

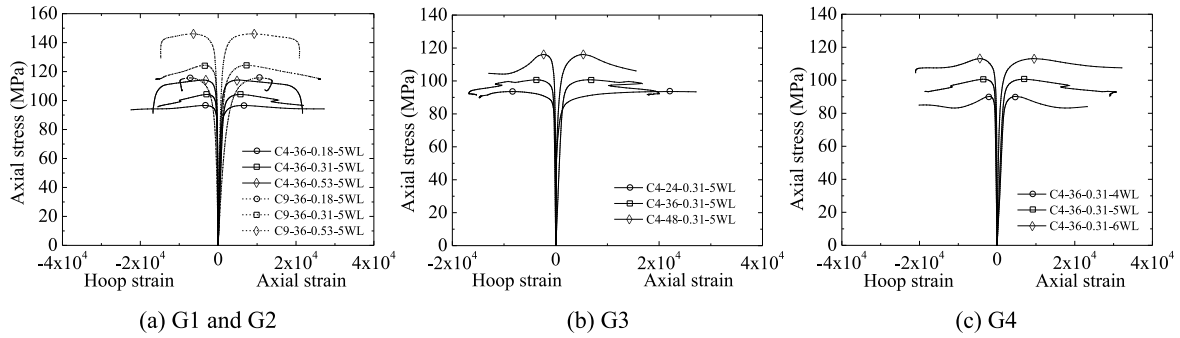


Fig. 4. Axial stress vs. strain curves of inner steel tubes.

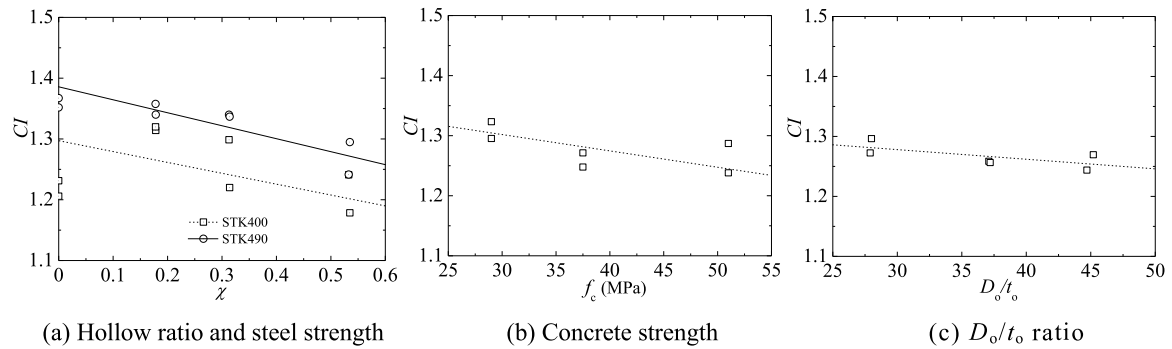


Fig. 5. Composite effects of the tested specimens.

$$Q = S_{\theta}^2 + S_z^2 + 2v_s S_{\theta} S_z + 2H(1 - v_s)\sigma_c^2 / (9G) \quad (10)$$

$$q = \frac{2H}{9E_s} \sigma_c^2 \quad (11)$$

in which H denotes the gradient of equivalent plastic stress–strain curve obtained from the tensile coupon tests of the steel tube; q denotes the equivalent stress variable; Q stands for the equivalent deviatoric stress variable [43]; G symbolizes the shear modulus, computed by $G = E_s / (2(1 + v_s))$; S_z and S_{θ} represent the deviatoric stresses in axial and circumferential directions, respectively, and they are computed by:

$$S_z = (2\sigma_z - \sigma_{\theta}) / 3 \quad (12)$$

$$S_{\theta} = (2\sigma_{\theta} - \sigma_z) / 3 \quad (13)$$

Accordingly, using Eqs. (5) to (13), the axial and circumferential stresses can be derived from the read axial/circumferential strain at each loading process. The axial stress σ_z and circumferential stress σ_{θ} of the steel tube at each loading process are substituted into Eqs. (2) to (4), the lateral confining stresses induced by the external and internal tubes as well as the axial compressive stress of the sandwiched concrete will be obtained. In the current paper, the compressive stress is assumed to be positive, naturally, the tensile stress is negative. Note that the

stress of steel tube computed by Eqs. (5) to Eq. (13) is average stress along the circumferential of the steel tube. Additionally, the CSP is an average of the two identical specimens from each subset.

A typical CSP graph of confined concrete in a circular CFDST column is presented in Fig. 7, in which the specimen C4-24-0.31-5WL is taken as an example. The corresponding axial stress versus axial or circumferential strain curves of the external and internal tubes are described in Fig. 8. From Fig. 7, it is clear that two different CSPs appear in CFDST columns owing to different confinement mechanisms of the external and internal tubes. Thereinto, the σ_{or} vs. f_{cz}/f_c curve represents the CSP induced by external tube, referred to as the ‘external CSP’, while the σ_{ir} vs. f_{cz}/f_c curve stands for the CSP yielded by internal tube, called the ‘internal CSP’.

First of all, for the external CSP, its characteristics are similar to the CSP of confined concrete in a CFST column previously reported by the authors [32,34]. Generally, the external CSP consists of four stages. For stage OA, due to the Poisson’s ratio of the steel tube larger than that of the concrete, the sandwiched concrete experiences no or less the lateral confining stress (σ_{or}). When the f_{cz}/f_c exceeds point A (about 0.65), the microcracks in the sandwiched concrete propagate rapidly, which results in the lateral expansion of concrete larger than that of

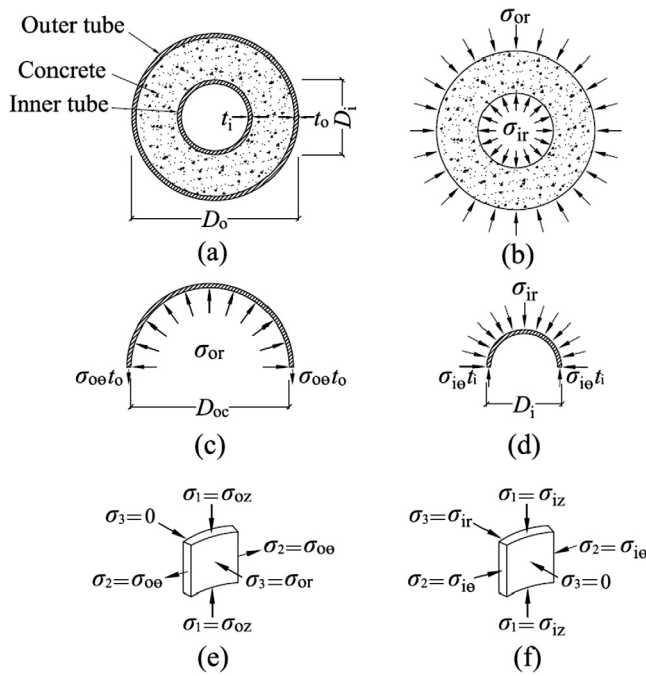


Fig. 6. Stress state between steel tubes and concrete.

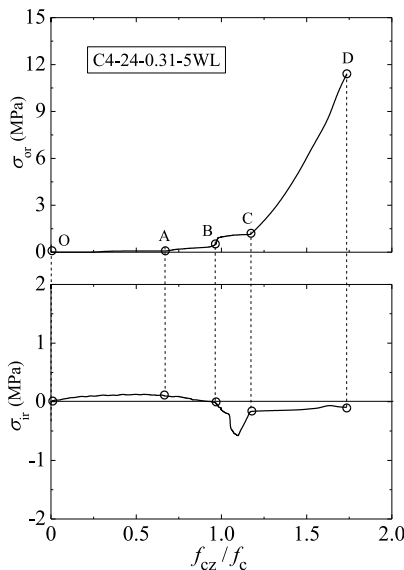


Fig. 7. CSPs of confined concrete in a CFDST column.

the steel tube. As a result, the lateral confining stress afforded to the sandwiched concrete raises smoothly. Then, an abrupt lateral expansion of the concrete owing to its fracture at point B triggers a sharp rise in the lateral confining stress. Subsequently, the steel tube yields at point C with increasing the value of f_{cz}/f_c . After undergoing a short plateau, owing to the strain hardening of steel tube, the lateral confining stress keeps raising and ends at the point D of the ultimate state. Generally, the stages OB and BD in the external CSP suggest that the concrete in a CFDST column experiences the pre- and post-fracture stages, which are similar to the state of concrete in a CFST column [32].

Secondly, different from the external CSP, the internal CSP exhibits insignificant change and mainly fluctuates around horizontal zero axis. Corresponding to the external CSP, the internal CSP also consists of four stages. For stage OA, owing to the Poisson's ratio of the steel tube larger than that of the concrete, the slight interaction between

the internal tube and the concrete is yielded. As a result, the internal tube provides a slight lateral confining stress (σ_{ir}) to the inner surface of the sandwiched concrete. When the f_{cz}/f_c exceeds point A, the microcracks in the sandwiched concrete propagate rapidly. As the axial compression continues, the lateral expansion rate of the inner surface of the sandwiched concrete is gradually greater than that of the internal tube. As a result, the lateral confining stress induced by the internal tube decreases smoothly to zero. Subsequently, due to the adhesion between the concrete and the outer surface of the internal tube, the lateral confining stress induced by the internal tube after point B becomes the lateral tensile stress until point D.

2.4. Evaluation index of CSPs

Three typical CSPs of concrete under different confining conditions, i.e., the paths P_0 (OB), P_i (OCG) and P_a (OAH), are illustrated in Fig. 9. Among them, the path P_0 (OB) is the CSP of the plain concrete, and the path P_a (OAH) stands for the CSP of the actively confined concrete. However, the path P_i (OCG) represents the CSP of the passively confined concrete. Such CSP is usually generated in the passively confining concrete structures, e.g., CFDST columns, FRP-confined concrete and steel-reinforced concrete (RC) columns. At the same time, the CSP of the confined concrete in FRP-confined concrete given by Lin et al. [33], indicated by the red curve, is also depicted in Fig. 9. From Fig. 9, it can be seen that the shape of the curve BCG of the two CSPs is different due to the different material properties of the two confining materials. The detailed elucidation for the three typical CSPs can be found in Ref. [33].

In the current paper, two assessment indices developed by the authors [32–34] were employed to quantify the performance of the CSPs and the relationship between the CSP and the concrete compressive strength.

First of all, the domination extent of the lateral confining stress in a CSP (P_i) is represented by a dominance index, which is determined by:

$$SI(P_i) = \frac{S(P_i)}{S(P_{i,up})} \quad (14)$$

in which $S(P_i)$ symbolizes the area enclosed by the paths P_i and $P_{i,low}$ (OEG). $S(P_{i,up})$ denotes the area enclosed by the paths $P_{i,up}$ (OAG) and $P_{i,low}$ (OEG). Noticeably, a larger value of SI means that the path P_i is closer to path P_a , which indicates that a more remarkable lateral confining stress is achieved. In other words, for CSP with a larger SI value, the lateral confining pressure stress acts a leading role in confining concrete.

It should be noted that a CSP P_i in a CFST column is only generated by the external steel tube, while two different CSPs in a CFDST column are induced by the external and internal tubes, respectively. Accordingly, in this paper, an equivalent lateral confining stress was suggested to represent the overall confinement effect of the external and internal tubes on confined concrete in a CFDST column. For instance, the lateral confining stress (σ_{rs}) in Fig. 9 is an equivalent stress, which is defined as the vector sum of the stresses σ_{or} and σ_{ir} induced by the external and internal tubes, respectively. According to Fig. 6, the expression of the equivalent stress σ_{rs} is determined by:

$$\sigma_{rs} = \sigma_{or} - \sigma_{ir} = \frac{-2\sigma_{oo}t_o}{D_o - 2t_o} - \frac{2\sigma_{io}t_i}{D_i} \quad (15)$$

Secondly, to assess the CSP effect on the compressive strength of confined concrete in a CFDST column, an effect index λ was introduced as:

$$\lambda(P_i) = \frac{\Delta f(P_i, \sigma_{ru})}{\Delta f(P_a, \sigma_{ru})} \quad (16)$$

in which, $\Delta f(P_i, \sigma_{ru})$ is the increment of the concrete strength under path P_i ; that is to say, $\Delta f(P_i, \sigma_{ru}) = f_{cc} - f_c$, where f_{cc} is the compressive strength of confined concrete; $\Delta f(P_a, \sigma_{ru}) = f_{ac} - f_c$, stands for the increment of the concrete strength under path P_a , and was taken as

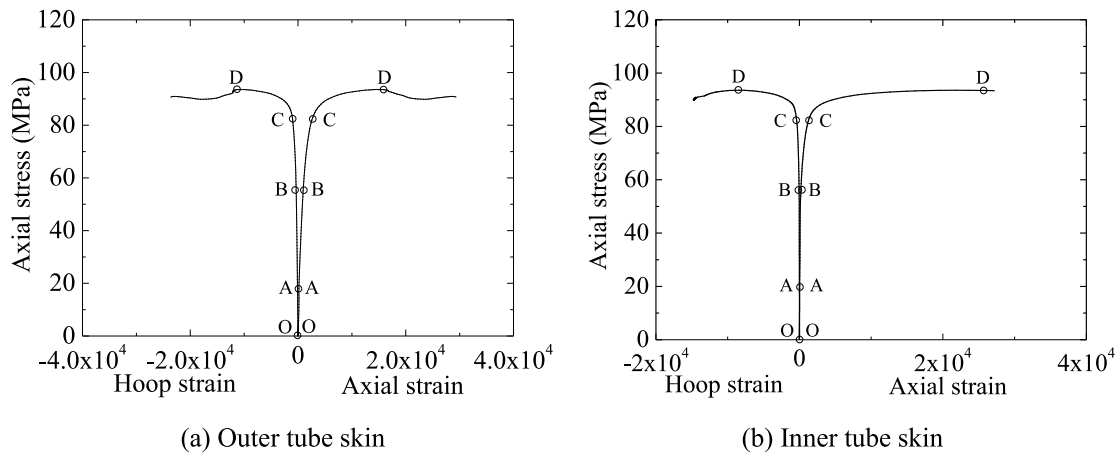


Fig. 8. Axial stress–strain curves for specimen C4-24-0.31-5WL.

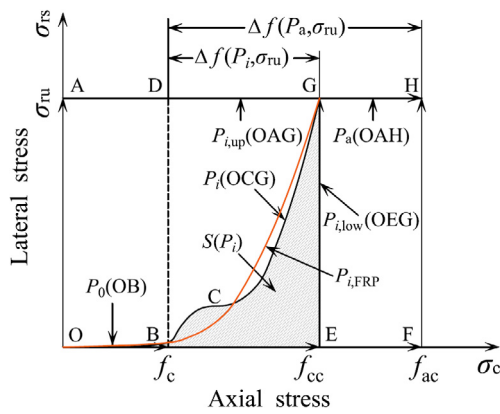


Fig. 9. Typical CSPs of concrete under different confining conditions. (For interpretation of the references to colour in this figure legend, the reader is referred to the web version of this article.)

2.2 $f_c^{0.3} \sigma_{ru}^{0.81}$ proposed by authors in Ref. [32]. Note that the CSP under path P_a is only affected by the ultimate lateral stress, i.e., $\Delta f(P_a, \sigma_{ru}) = \Delta f(\sigma_{ru})$ [33]. Accordingly, Eq. (16) can be rewritten as

$$\lambda(P_i) = \frac{\Delta f(P_i, \sigma_{ru})}{\Delta f(\sigma_{ru})} \quad (17)$$

In Eq. (17), $\lambda \neq 1.0$ means the increments of the concrete strength under different CSPs are different, which suggests that the compressive strength of confined concrete is CSP-dependent. The larger the deviation between the λ value and unity, the more remarkable the CSP effect. Instead, $\lambda = 1.0$, i.e., $\Delta f(P_i, \sigma_{ru}) = \Delta f(\sigma_{ru})$, means that the increments of the concrete strength under different CSPs are same, which demonstrates that the CSP makes little contribution to the change of concrete strength (i.e., so called CSP-independent).

3. Investigation of confining stress path (CSP)

In this section, the CSPs of the CFDST columns with different column variables and their corresponding effects are investigated.

3.1. Parametric analysis on CSP

3.1.1. Effects of χ ($\chi = D_i/D_o$) on CSP

The external and internal CSPs of confined concrete in circular CFDST columns with different χ values are shown in Fig. 10. From this figure, it can be found that the parts of the external CSPs in the pre-fracture (OAB) stage are almost similar, while the obvious

differences are found in the post-fracture (BCD) stage. That is, the hollow ratio considerably affects the parts of the CSPs in the post-fracture (BCD) stage. The CSP in specimens with larger χ tends to generate a lower BC stage with a shorter plateau, and a steeper CD stage. This indicates that higher hollow ratio provides a weaker lateral confinement effect and acts an insignificant role in delaying concrete fracture. Additionally, Fig. 10 also shows that the internal CSPs with different χ values fluctuate around abscissa axis with inapparent trend. This suggests that the hollow ratio has little effect on the internal CSPs, and internal tube provides less confinement effect to the sandwiched concrete. Accordingly, the effects of the yield stress and diameter-to-thickness ratio of internal tube on the CSPs will not be further discussed in the next sections.

3.1.2. Effects of f_{syo} on CSP

The effects of f_{syo} on the external CSPs of confined concrete in circular CFDST columns were examined against the test results of G1 and G2 specimens. The CSPs of the specimens with different f_{syo} values are shown in Fig. 11. From this figure, it can be seen that the external tube yield stress significantly affects the parts of the CSPs in the pre-fracture (OAB) and post-fracture (BCD) stages. Compared with different f_{syo} values, the lateral stress in the specimens with a higher f_{syo} value appears in an earlier stage, thus achieving a shorter OA part and a longer AB part. Additionally, the CSP in the specimens with a higher f_{syo} value tends to achieve a higher BC part with a longer plateau, and a longer and gentler CD part. This suggests that the specimens with a higher f_{syo} value exhibit better ductility performance due to higher confinement effect. This finding is consistent with that in axially loaded CFST column reported by the authors [32].

3.1.3. Effects of f_c on CSP

The external and internal CSPs of confined concrete in the CFDST columns with different f_c values are shown in Fig. 12. From this figure, it can be seen that the OABC parts of the external CSPs are similar, while only difference is found in the CD parts of the external CSPs. This indicates that the concrete strength remarkably influences the CD part of the external CSPs during the strain hardening stage of the external tube. The CFDST column filled with a higher f_c value tends to achieve a shorter and steeper CD part. This suggests that the higher strength concrete undergoes a weaker lateral confinement effect under the identical confinement conditions, which is mainly attributed to the brittleness of high-strength concrete. However, the concrete strength affords less contribution to the internal CSPs. Also, the inner tube provides an insignificant lateral confinement effect to the concrete infill, which is consistent with the observation in Section 3.1.1.

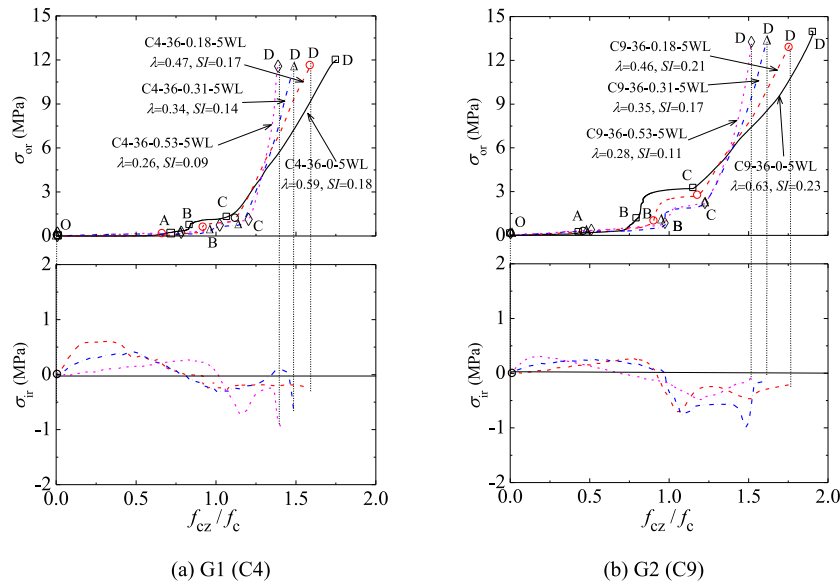


Fig. 10. CSPs for specimens with different χ values.

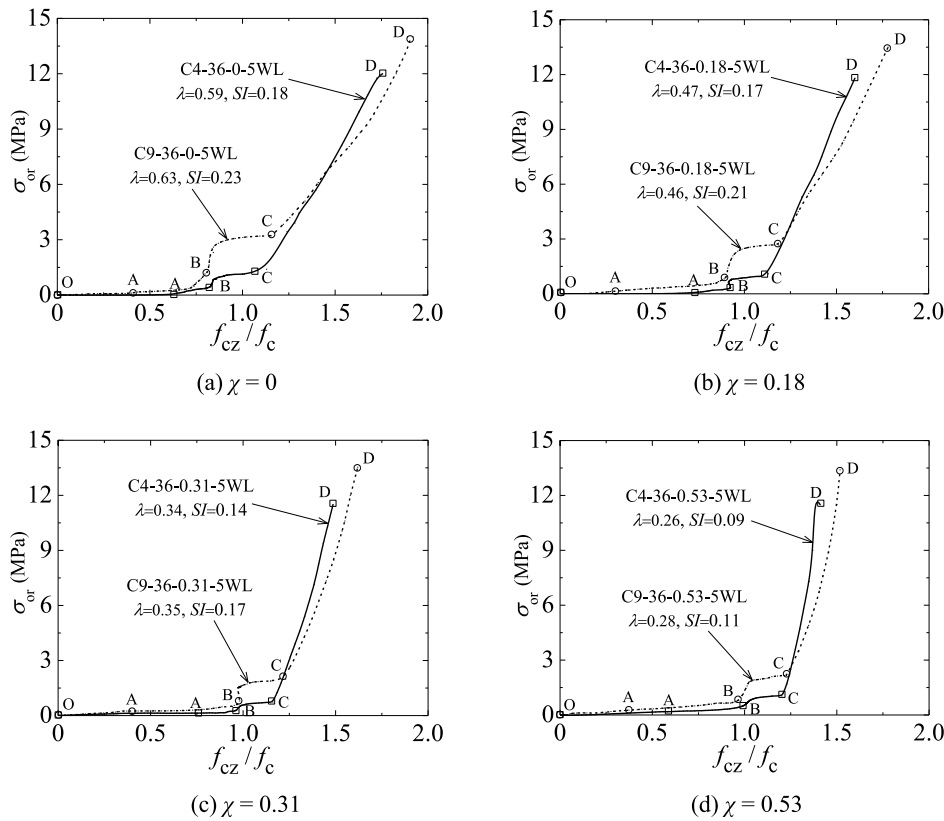


Fig. 11. CSPs for specimens with different f_{sy0} values.

3.1.4. Effects of D_o/t_o ratio on CSP

The external and internal CSPs of confined concrete in the CFDST columns with different D_o/t_o ratios are shown in Fig. 13. From this figure, it can be found that the D_o/t_o ratio yields an insignificant effect on the OABC parts of the external CSPs. Only difference is found in the length of the CD parts of the external CSPs, in which the external tube is in the strain hardening state. CFDST columns with a larger D_o/t_o ratio tend to generate a shorter CD part. This shows that the outer steel tubes with a larger D_o/t_o ratio provide a weaker lateral confinement effect, resulting in a lower ultimate axial load and ductility

of the column. Additionally, the findings similar to Sections 3.1.1 and 3.1.3 were observed in this section for the internal CSPs.

As discussed above, the OB part (the pre-fracture stage of concrete infill) of the external CSP is only influenced by f_{sy0} , while the BC part of the external CSP is affected by both χ and f_{sy0} . However, the CD part of the external CSP is almost influenced by all the examined column parameters. Different from the external CSP, the internal CSP is hardly affected by χ , f_{sy0} , f_c and D_o/t_o ratio. Generally, the column parameters investigated yield significant effects on the external CSP, but less effects on the internal CSP.

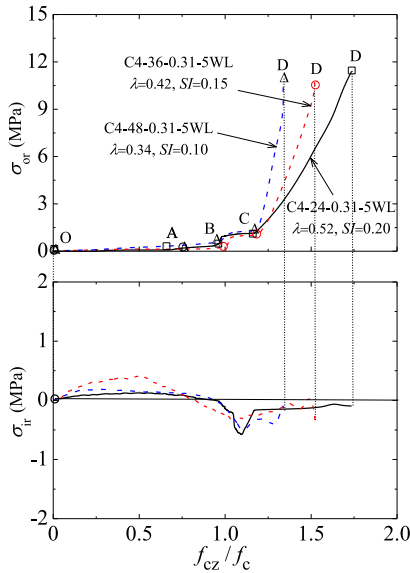


Fig. 12. CSPs for specimens with different f_c values.

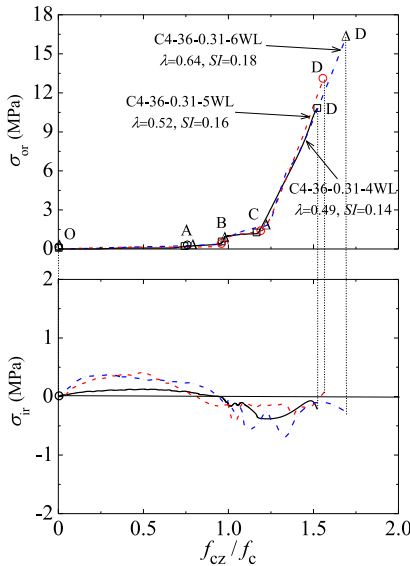


Fig. 13. CSPs for specimens with different D_o/t_o ratios.

3.1.5. Relationship between SI and CSP

As defined above, the CSP of confined concrete in circular CFDST columns is represented by the domination index SI , calculated by

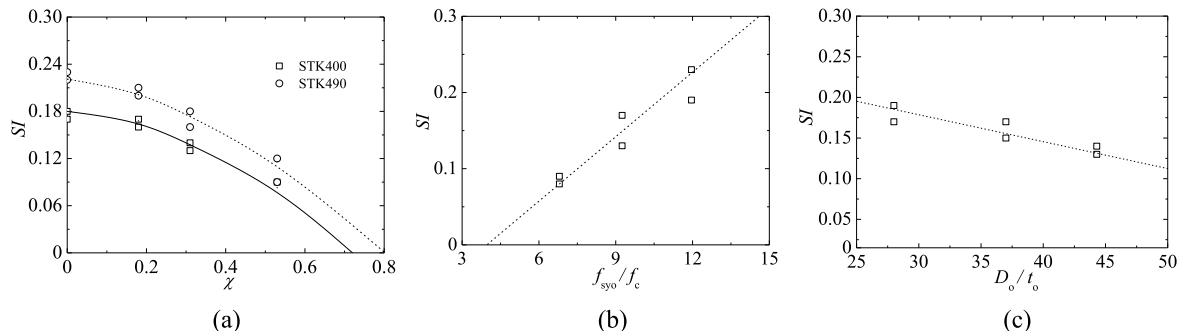


Fig. 14. Relationships between laterally dominant index and variables investigated.

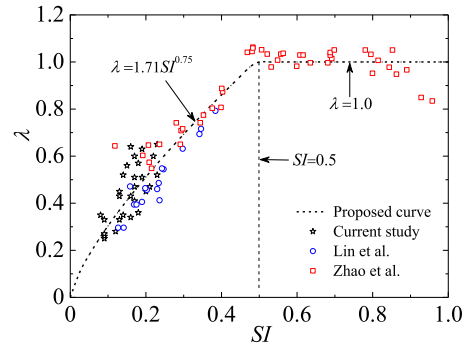


Fig. 15. Relationship between effect index λ and domination index SI .

Eq. (14). The values of SI for all the specimens are listed in Table 1. The mean value of SI for two identical specimens is also given in Figs. 10 to 13 for the corresponding CSP. Since the external CSPs are influenced by χ , f_{sy0} , f_c and D_o/t_o ratio, the domination index SI should be quantitatively expressed by these variables. The relationships between the domination index SI and column parameters, i.e., SI vs. χ , SI vs. f_{sy0}/f_c and SI vs. D_o/t_o ratio, are shown in Fig. 14. The domination index SI decreases as the χ and D_o/t_o ratio increase, while it increases as the f_{sy0}/f_c increases. This demonstrates that with increasing χ , f_c and D_o/t_o ratio, the CSP gets closer to the path P_0 , which suggests that the lateral confining stress acts an insignificant role in the external CSP. On the contrary, with increasing f_{sy0} , the CSP gets closer to the path P_a , which implies that the lateral confining stress acts a vital role in the external CSP.

3.2. CSP effect on the compressive strength

In this section, the influences of CSPs on the compressive strength of confined concrete are discussed. As defined above, such effect is characterized by an effect index λ ; see Eq. (17). The values of λ for all the specimens are listed in Table 1, and the average value of λ from the two identical specimens is also shown in Figs. 10 to 13. It can be found that all the effect indices fall between 0 and 1. The reason for this is the equivalent CSPs of confined concrete in circular CFDST columns shift between those of the plain concrete and actively confined concrete. That is, the compressive strength (f_{cc}) of confined concrete in CFDST columns varies between f_c and f_{ac} , i.e., $f_{cc} \in (f_c, f_{ac})$.

The relationship between the effect index λ and domination index SI is depicted in Fig. 15. In general, (a) the effect index λ for circular CFDST columns is smaller than the unity, i.e., $\lambda \neq 1.0$, which indicates that the compressive strength of confined concrete in circular CFDST columns is CSP-dependent; (b) the effect index λ is generally improved as the domination index SI raises. This indicates that the CSP for CFDST column with a smaller SI yields more significant impact on the compressive strength of confined concrete. That is, the CSP effect

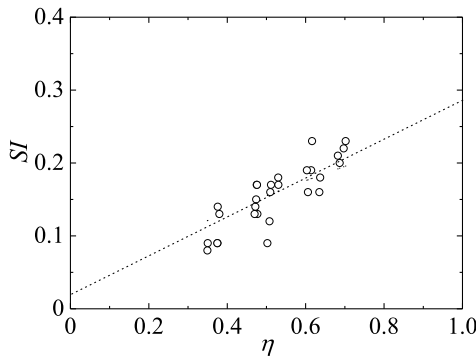


Fig. 16. Relationship between SI and η .

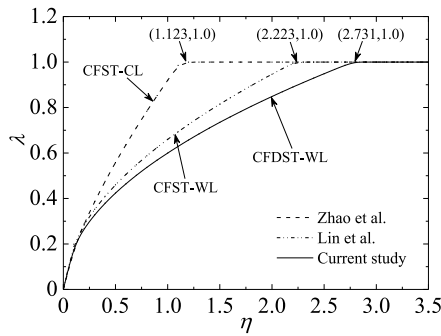


Fig. 17. Effect index vs. confinement coefficient curves.

on the behaviour of confined concrete is more significant when the confinement effect is weaker.

It should be noted that the values of SI of the current study fall into the interval of (0.08, 0.23), for the purpose of generality, the values of the two indices λ and SI for circular CFST columns provided by Zhao et al. [32] and Lin et al. [34] are also depicted in Fig. 15. The compressive strength of confined concrete is CSP-dependent for $SI \in (0, 0.5)$, while it is CSP-independent for $SI \in [0.5, 1]$. The relationship between the two indices λ and SI generally follows the observations given by Zhao et al. [32] and Lin et al. [34], a lightly modified model is proposed to interpret their relationship, as given in Eq. (18). The proposed model is expressed in the form of a dash line in Fig. 15. From this figure, it can be seen that, in general, the test results of the current and previous studies are evenly distributed on both sides of the dash line.

$$\lambda = \begin{cases} 1.71SI^{0.75} & , 0 \leq SI < 0.5 \\ 1.0 & , 0.5 \leq SI \leq 1.0 \end{cases} \quad (18)$$

From Eq. (18), it can be noticed that once the domination index SI is determined, the value of the effect index λ will be obtained. As stated above, the domination index SI is influenced by the column parameters, i.e., χ , f_{sy0} , f_c and D_o/t_o ratio. To reflect such effect, a confinement coefficient η considering these variables is defined as:

$$\eta = (1 - \chi^2) \frac{2t_o}{D_o - 2t_o} \frac{f_{sy0}}{f_c} \quad (19)$$

The relationship between η and SI is illustrated in Fig. 16. Based on the regression analysis of the test results, a model reflecting such relationship is proposed as:

$$SI = 0.25\eta^{0.69} \quad (20)$$

Then, by substituting Eq. (20) into Eq. (18), Eq. (18) becomes the following equation:

$$\lambda_{CFDST} = \begin{cases} 0.60\eta^{0.51} & , 0 \leq \eta < 2.731 \\ 1.0 & , 2.731 \leq \eta \leq 7.457 \end{cases} \quad (21)$$

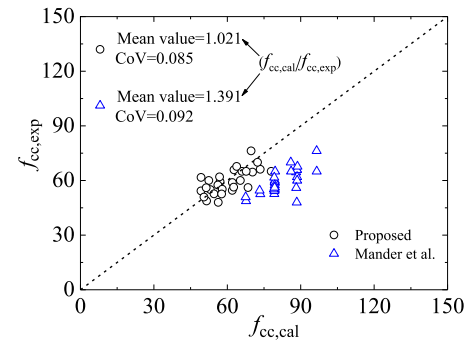


Fig. 18. Verification of the developed model.

In order to well understand the confinement effects of circular CFDST and CFST columns, the relationships between the effect index λ and confinement coefficient η from such columns are depicted in Fig. 17. In Fig. 17, ‘WL’ indicates that the full section of the column is subjected to axial load, ‘CL’ denotes that only the concrete section of the column is subjected to axial load. From Fig. 17, it can be observed that:

(I) Similar to CFST columns, the effect indices of CFDST columns with η falling between 0 and 2.731 are smaller than the unity, which suggests that the compressive strength of confined concrete in CFDST columns with η less than 2.731 is CSP-dependent.

(II) In general, the effect indices of CFDST column are less than those of CFST columns under different loading conditions, which implies that the confinement effects of CFDST columns are weaker than those of CFST columns. Note that when the η is smaller than about 0.2, the effect indices of CFDST and CFST columns are almost the same, which demonstrates that the confinement effects for both are almost identical. It is probably because columns with a smaller η (i.e., larger χ and D/t ratios (lead to premature buckling) or lower strength ratio f_y/f_c) have generally experienced a lower axial stress of steel tube, resulting in a higher circumferential stress of steel tube (according to the von Mises yield criterion).

(III) As the η increases, the effect indices of CFST and CFDST columns become the unity in turn, which suggests that the confinement effects for both are identical. Also, the compressive strength of confined concrete in columns with a larger η ($\eta \geq 2.731$) is CSP-independent.

Furthermore, based on Eq. (17), a compressive strength model of confined concrete in CFDST columns considering the CSP effect is given by:

$$f_{cc} = f_c + 2.2\lambda f_c^{0.3} \sigma_{ru}^{0.81} \quad (22)$$

$$\sigma_{ru} = \sigma_{or,u} - \sigma_{ir,u} = \frac{-2\sigma_{o\theta,m}t_o}{D_o - 2t_o} - \frac{2\sigma_{i\theta,m}t_i}{D_i} \quad (23)$$

where $\sigma_{o\theta,m}$ and $\sigma_{i\theta,m}$ symbolize the circumferential stresses of the external and internal tubes at the maximum axial load, respectively. It should be that the proposed model in this paper is not only applicable to CSP-dependent but also to CSP-independent. When the confined concrete in CFDST columns is CSP-independent, the value of λ in Eq. (22) is taken as 1.

In order to examine the performance of the developed model, comparisons between the results calculated by the developed and previous models and the measured values are shown in Fig. 18. From this figure, it can be seen that the mean value and coefficient of variation (CoV) from the developed model are 1.021 and 0.085, respectively, while for the model suggested by Mander et al. [31], they are 1.391 and 0.092, respectively. This demonstrates that a higher prediction performance is achieved in the developed model. Simultaneously, it should be noted that the developed model can also be suitably applied to predict the compressive strength of confined concrete in circular CFST columns by setting the hollow ratio (χ) to 0.

4. Proposal of compressive strength model for CFDST columns

4.1. Basic consideration for model

In this section, based on the confined concrete model developed in Section 3.2, a compressive strength model for estimating the cross-sectional resistances of CFDST columns is proposed. To this end, Eq. (4) in Section 2.3 is rewritten as:

$$N_m = \sigma_{oz,m} A_{os} + f_{cz,m} A_{sc} + \sigma_{iz,m} A_{is} \quad (24)$$

where $\sigma_{oz,m}$ and $\sigma_{iz,m}$ symbolize the axial stresses of the external and internal tubes at the maximum axial load, respectively; $f_{cz,m}$ represents the concrete compressive stress at the maximum axial load, i.e., $f_{cz,m} = f_{cc}$. Therefore, according to Eq. (24), once $\sigma_{oz,m}$, $\sigma_{iz,m}$ and f_{cc} is determined, the maximum axial load N_m can be obtained.

In order to obtain the value of f_{cc} , the determination of σ_{ru} is a prerequisite. As defined above, the equivalent ultimate lateral stress σ_{ru} in Eq. (23) is calculated only by experimental axial and circumferential strains according to the generalized Hooke's Law and the incremental Prandtl-Reuss equation, which results in the time-consuming in calculations. Also, in some cases, the strains of the columns are not given. Moreover, the above investigation shows that the equivalent ultimate lateral stress σ_{ru} comes mainly from the external tube, and the contribution of the internal tube is meaningless. Hence, the ultimate lateral stress σ_{ru} in Eq. (23) can be rewritten as:

$$\sigma_{ru} = \frac{-2\sigma_{o\theta,m}t_o}{D_o - 2t_o} \quad (25)$$

Since the external tube is a thin-walled element in a bi-axial stress state, which meets the von Mises yield criterion as:

$$\sigma_{oz,m}^2 - \sigma_{oz,m}\sigma_{o\theta,m} + \sigma_{o\theta,m}^2 = \sigma_{oe,m}^2 \quad (26)$$

in which $\sigma_{oe,m}$ is the equivalent stress of external tube at the maximum axial load. In the current paper, $\sigma_{oe,m}$ is taken as μf_{sy0} . Using Eqs. (5) to (13), the values of μ for all the specimens are listed in Table 1. Here, the average value of μ will be employed, and taken as 1.045.

Supposing that the circumferential stress $\sigma_{o\theta,m}$ and the axial stress $\sigma_{oz,m}$ of the external tube at the maximum axial load are expressed by:

$$\sigma_{o\theta,m} = \alpha_o f_{sy0} \quad (27)$$

$$\sigma_{oz,m} = \beta_o f_{sy0} \quad (28)$$

where α_o and β_o denote the ratios of the circumferential and axial stresses to the external tube yield stress (f_{sy0}), respectively, similar to the suggestion of Liang and Fragomeni [48]. Substituting Eqs. (27) and (28) into Eq. (26), the expression becomes

$$\alpha_o^2 - \alpha_o\beta_o + \beta_o^2 = \mu^2 \quad (29)$$

According to Japanese standard AIJ [49], in this paper, α_o is taken as -0.19 . As a result, β_o can be determined by:

$$\beta_o = \frac{\alpha_o + \sqrt{4\mu^2 - 3\alpha_o^2}}{2} = 0.94 \quad (30)$$

Accordingly, using Eqs. (25) to (30), the value of f_{cc} in Eq. (22) would be obtained directly. Subsequently, by substituting Eqs. (22) and (28) into Eq. (24), Eq. (24) becomes:

$$N_m = 0.94 f_{sy0} A_{os} + A_{sc} f_{cc} + \sigma_{iz,m} A_{is} \quad (31)$$

In this paper, the maximum axial stress ($\sigma_{iz,m}$) of the internal tube is assumed to be f_{syi} . Therefore, N_m is finally determined by:

$$N_m = 0.94 f_{sy0} A_{os} + A_{sc} f_{cc} + f_{syi} A_{is} \quad (32)$$

4.2. Verification of the proposed model

In this section, the experimental results of the current and previous studies were collected and employed to evaluate the accuracy of the proposed and existing models. In total, 154 data from the tested columns were collected by the authors and their details can be found in Ref. [50], and a general summary is shown in Table 3. The effect indices λ for all the specimens are also listed in Table 3. It can be seen from this table that all λ values are less than the unity, which indicates that the collected CFDST specimens are CSP-dependent. In addition, the collected experimental data achieves a wide range of column variables, and their limitations are described as follows:

- (1) The hollow ratio χ (D_i/D_o) varies from 0 to 0.89;
- (2) The unconfined concrete strength (f_c) ranges from 18.7 MPa to 141.0 MPa;
- (3) The diameter-to-thickness ratios of the external and internal tubes range from 18.7 to 176.7 and 10.5 to 146.0, respectively;
- (4) The yield strengths of the external and internal tubes range from 221.0 MPa to 618.0 MPa and 216.0 MPa to 520.0 MPa, respectively.

Using the test data listed in Table 3, comparisons between the experimental strengths and the predictions by the proposed and existing models are shown in Table 4. From this table, it can be seen that Han et al. [6] underestimates the cross-sectional resistances of the CFDST columns, while Hassanein and Kharoob [27], Uenaka et al. [19], and Liang [29] overestimate the cross-sectional resistances of the CFDST columns. The average value of the proposed model is 0.930 with smaller standard deviation (SD) and CoV than the existing models. Generally, the proposed model can effectively predict the cross-sectional resistances of circular CFDST short columns made with a wide-range of column variables.

5. Conclusions

In this paper, the CSPs of CFDST columns were firstly investigated through axial compression tests. Two different CSPs of confined concrete induced by the external and internal steel tubes were presented. An equivalent lateral confining stress reflecting the confinement effects of the external and internal steel tubes to the concrete infill was defined. The two performance indices (i.e., the lateral stress domination index SI and the effect index λ) were introduced to quantitatively evaluate the CSPs and their effects on the compressive strength of confined concrete. Based on the scope of current study, the following findings were listed:

- The external CSPs of CFDST columns are remarkably affected by the column variables, i.e., χ , f_{sy0} , f_c and D_o/t_o ratio, but less effects on the internal CSPs.
- Similar to CFST columns, the effect indices of CFDST columns with η falling between 0 and 2.731 are less than the unity, which suggests that the compressive strength of confined concrete in the CFDST columns with η less than 2.731 is CSP-dependent.
- The effect indices of CFDST column are generally less than those of CFST columns, which implies that the confinement effects of CFDST columns are weaker than those of CFST columns. Note that when the η is smaller than about 0.2, the effect indices of CFDST and CFST columns are almost the same, which implies that the confinement effects for both are almost identical.
- As the η raises, the effect indices of CFST and CFDST columns become the unity in turn, which suggests that the confinement effects for both are identical. In other words, the compressive strength of confined concrete in the CFDST columns with η larger than 2.731 is CSP-independent.
- A CSP-based compressive strength model of axially compressed circular CFDST short columns is proposed, and a comparison with existing models indicates that a higher degree of accuracy and consistency of the predictions is achieved for the proposed model.

Table 3
Summary of tested CFDST short columns with circular carbon steel section.

Refs.	Number	D_o (mm)	t_o (mm)	D_i (mm)	t_i (mm)	χ (D_i/D_o)	f_{syo} (MPa)	f_{syt} (MPa)	f_c (MPa)	L (mm)	λ
Current study	28	187.7–191.0	4.21–6.77	33.5–101.6	3.06–4.10	0.00–0.53	327.3–464.0	342.1–348.2	29.0–51.0	570.1	0.25–0.65
Tao et al. [16]	12	114.0–300.0	3.00	48.0–165.0	3.00	0.27–0.78	275.9–294.5	294.5–396.1	39.7	372.0–900.0	0.18–0.33
Li et al. [13]	2	350.0	3.82	231.0	2.92	0.66	439.3	396.5	44.4	1050.0	0.21
Lin and Tsai [7]	2	300.0	2.00–4.00	180.0	2.00	0.60	290.0	290.0	22.4	900.0	0.20–0.28
Uenaka et al. [19]	9	157.0–159.0	0.90–2.14	38.0–115.0	0.90–2.14	0.24–0.73	221.0–308.0	221.0–308.0	18.7	471.0–477.0	0.15–0.38
Li and Cai [23]	4	356.0	5.50	168.0–219.0	3.30	0.47–0.62	618.0	356.0	38.8	1068.0	0.33–0.37
Ekmekyapar and Hasan [21]	8	114.3	2.73–5.85	60.3	2.52–5.77	0.53	285.0–455.0	310.0–396.0	38.6–64.6	343.0	0.24–0.59
Zhao et al. [12]	6	114.2–165.3	2.90–5.90	48.4–101.8	2.80–3.10	0.42–0.62	395.0–454.0	410.0–425.0	60.9	343.0–496.0	0.23–0.50
Wei et al. [28]	26	74.7–114.3	0.59–1.78	61.2–88.9	0.55–1.56	0.56–0.83	255.0–524.0	216.0–512.0	58.6	224.0–343.0	0.09–0.22
Fan et al. [51]	8	240.0	3.00–4.00	80.0–120.0	3.00–4.00	0.33–0.50	280.0	280.0	29.0	720.0	0.25–0.32
Ekmekyapar et al. [52]	8	114.3	2.74–6.11	60.3	2.52–5.77	0.53	355.0	310.0–396.0	41.2–68.2	343.0	0.26–0.64
Sulthana and Jayachandran [53]	2	166.0–166.3	5.22–5.24	76.7	3.58	0.46	520.0	520.0	34.6–35.4	450.0	0.53
Li et al. [54]	6	140.0–450.0	2.50–8.00	76.0–400.0	1.60–8.00	0.54–0.89	307.0–365.0	321.0–429.0	41.2–44.5	420.0–1350.0	0.15–0.26
Zhao et al. [55]	9	114.3–165.1	1.70–6.00	48.3–101.6	2.90–3.30	0.42–0.63	395.0–454.0	394.0–425.0	60.9	343.0–495.0	0.17–0.51
Yan et al. [50]	24	164.7–165.3	3.68–6.02	42.5–76.4	2.78–3.21	0.26–0.46	347.0–428.6	385.6–409.8	53.7–141.0	570.0	0.18–0.42

Table 4
Means and CoVs of all test strengths-to-predicted strengths.

Design models	Han et al. [6]	Uenaka et al. [19]	Hassanein and Kharoob [27]	Liang [29]	Proposed model
154 test data	$N_{u,c}/N_{u,e}$	$N_{u,c}/N_{u,e}$	$N_{u,c}/N_{u,e}$	$N_{u,c}/N_{u,e}$	$N_{u,c}/N_{u,e}$
Mean	0.915	1.157	1.064	1.021	0.930
SD	0.106	0.120	0.119	0.274	0.091
CoV	0.115	0.103	0.112	0.269	0.098

CRedit authorship contribution statement

Xi-Feng Yan: Conceptualization, Methodology, Data curation, Investigation, Writing - review & editing, Validation. **Yan-Gang Zhao:** Supervision, Review, Funding acquisition, Project administration. **Siqi Lin:** Data curation, Supervision, Review, Funding acquisition. **Haizhong Zhang:** Validation, Review, Supervision.

Declaration of competing interest

The authors declare that they have no known competing financial interests or personal relationships that could have appeared to influence the work reported in this paper.

Data availability statement

Part or all data used, models will be available from the first author based on reasonable request.

Acknowledgements

The research described in this paper is partially supported by the National Science Foundation of China (Grant No. 51738001, 52008009), China Postdoctoral Science Foundation (Grant No. 2020M670076), and Beijing Postdoctoral Research Foundation, China (Grant No. Q6004013202001). The supports are greatly appreciated by the authors.

References

[1] X.F. Yan, Y.G. Zhao, Compressive strength of axially loaded circular concrete-filled double-skin steel tubular short columns, *J. Constr. Steel Res.* 170 (2020) 106114.
 [2] F.Y. Wang, B. Young, L. Gardner, Experimental study of square and rectangular CFDST sections with stainless steel outer tubes under axial compression, *J. Struct. Eng.* 145 (11) (2019) 04019139.
 [3] L.H. Han, W. Li, R. Bjorhovde, Developments and advanced applications of concrete-filled steel tubular (CFST) structures: members, *J. Constr. Steel Res.* 100 (2014) 211–228.
 [4] Y.G. Zhao, X.F. Yan, S.Q. Lin, Compressive strength of axially loaded circular hollow centrifugal concrete-filled steel tubular short columns, *Eng. Struct.* 201 (2019) 109828.
 [5] H. Huang, L.H. Han, Z. Tao, X.L. Zhao, Analytical behavior of concrete-filled double skin steel tubular (CFDST) stub columns, *J. Constr. Steel Res.* 66 (3) (2010) 542–555.

[6] L.H. Han, Z. Tao, H. Huang, X.L. Zhao, Concrete-filled double-skin (SHS outer and CHS inner) steel tubular beam–columns, *Thin-Walled Struct.* 42 (9) (2004) 1329–1355.
 [7] M.L. Lin, K.C. Tsai, Behavior of double-skinned composite steel tubular columns subjected to combined axial and flexural loads, in: *Proceedings of the First International Conference on Steel and Composite Structures*, 2001, pp. 1145–1152.
 [8] Y. Yagishita, H. Kitoh, M. Suimoto, T. Tanihira, K. Sonoda, Double skin composite tubular columns subjected to cyclic horizontal force and constant axial force, in: *Conference Proceedings of the 6th International Conference on Steel and Concrete Composite Structures Held in USA*.
 [9] R. Imani, G. Mosqueda, M. Bruneau, Finite element simulation of concrete-filled double-skin tube columns subjected to postearthquake fires, *J. Struct. Eng.* 141 (12) (2015) 04015055.
 [10] M. Ahmed, J.C. Ci, X.F. Yan, S.Q. Lin, S.C. Chen, Numerical modeling of axially loaded circular concrete-filled double-skin steel tubular short columns incorporating a new concrete confinement model, *Struct.* 30 (2021) 611–627.
 [11] X.F. Yan, Y.G. Zhao, Experimental and numerical studies of circular sandwiched concrete axially loaded CFDST short columns, *Eng. Struct.* 230 (2021) 111617.
 [12] X.L. Zhao, R. Grzebieta, M. Elchalakani, Tests of concrete-filled double skin CHS composite stub columns, *Steel Compos. Struct.* 2 (2) (2002) 129–146.
 [13] W. Li, Q.X. Ren, L.H. Han, X.L. Zhao, Behaviour of tapered concrete-filled double skin steel tubular (CFDST) stub columns, *Thin-Walled Struct.* 57 (2012) 37–48.
 [14] F.C. Wang, L.H. Han, W. Li, Analytical behavior of CFDST stub columns with external stainless steel tubes under axial compression, *Thin-Walled Struct.* 127 (2018) 756–768.
 [15] Y.F. Yang, L.H. Han, B.H. Sun, Experimental behavior of partially loaded concrete filled double-skin steel tube (CFDST) sections, *J. Constr. Steel Res.* 71 (2012) 63–73.
 [16] Z. Tao, L.H. Han, X.L. Zhao, Behavior of concrete-filled double skin (CHS inner and CHS outer) steel tubular stub columns and beam columns, *J. Constr. Steel Res.* 60 (8) (2004) 1129–1158.
 [17] V.I. Patel, Q.Q. Liang, Muhammad NSH, Numerical analysis of circular double-skin concrete-filled stainless steel tubular short columns under axial loading, *Struct.* 24 (2020) 754–765.
 [18] M.F. Hassanein, O.F. Kharoob, L. Gardner, Behaviour and design of square concrete-filled double skin tubular columns with inner circular tubes, *Eng. Struct.* 100 (2015) 410–424.
 [19] K. Uenaka, H. Kitoh, K. Sonoda, Concrete filled double skin circular stub columns under compression, *Thin-Walled Struct.* 48 (2010) 19–24.
 [20] Y. Essopjee, M. Dundu, Performance of concrete-filled double skin circular tubes in compression, *Compos. Struct.* 133 (2015) 1276–1283.
 [21] T. Ekmekyapar, H.G. Hasan, The influence of the inner steel tube on the compression behavior of the concrete filled double skin steel tube (CFDST) columns, *Mar. Struct.* 66 (2019) 197–212.
 [22] F.Y. Wang, B. Yong, L. Gardner, Compressive testing and numerical modelling of concrete-filled double skin CHS with austenitic stainless steel outer tubes, *Thin-Walled Struct.* 141 (2019) 345–359.
 [23] W. Li, Y.X. Cai, Performance of CFDST stub columns using high-strength steel subjected to axial compression, *Thin-Walled Struct.* 141 (2019) 411–422.

- [24] H.T. Hu, F.C. Su, Nonlinear analysis of short concrete-filled double skin tube columns subjected to axial compressive forces, *Mar. Struct.* 24 (2011) 319–337.
- [25] T.T. Le, V.I. Patel, Q.Q. Liang, P. Huynh, Axisymmetric simulation of circular concrete-filled double-skin steel tubular short columns incorporating outer stainless-steel tube, *Eng. Struct.* 227 (2021) 111416.
- [26] M.F. Hassanein, O.F. Kharoob, Q.Q. Liang, Circular concrete-filled double skin tubular short columns with external stainless steel tubes under axial compression, *Thin-Walled Struct.* 73 (2013) 252–263.
- [27] M.F. Hassanein, O.F. Kharoob, Compressive strength of circular concrete-filled double skin tubular short columns, *Thin-Walled Struct.* 77 (2014) 165–173.
- [28] S. Wei, S.T. Mau, C. Vipulanandan, S.K. Mantrala, Performance of new sandwich tube under axial loading: Experiment, *J. Struct. Eng.* 121 (12) (1995) 1806–1814.
- [29] Q.Q. Liang, Nonlinear analysis of circular double-skin concrete-filled steel tubular columns under axial compression, *Eng. Struct.* 131 (15) (2017) 639–650.
- [30] F.E. Richart, A. Brandtzaeg, A. Brown, A study of the failure of concrete under combined compressive stresses, in: *Bulletin No. 185*, University of Illinois, Engineering Experimental Station, Champaign (IL, USA), 1928.
- [31] J.B. Mander, M.J.N. Priestley, R. Park, Theoretical stress-strain model for confined concrete, *J. Struct. Eng.* 114 (1988) 1804–1826.
- [32] Y.G. Zhao, S.Q. Lin, Z.H. Lu, T. Saito, L.S. He, Loading paths of confined concrete in circular concrete loaded CFT stub columns subjected to axial compression, *Eng. Struct.* 156 (2018) 21–31.
- [33] S.Q. Lin, Y.G. Zhao, J.M. Li, Z.H. Lu, Confining stress path based compressive strength model of axially loaded FRP-confined columns, *J. Compos. Constr.* 25 (1) (2021) 04020077.
- [34] S.Q. Lin, Y.G. Zhao, L.S. He, Stress paths of confined concrete in axially loaded circular concrete-filled steel tube stub columns, *Eng. Struct.* 173 (2018) 1019–1028.
- [35] I. Imran, S.J. Pantazopoulou, Experimental study of plain concrete under triaxial stress, *ACI Mater. J.* 93 (1996) 589–601.
- [36] X.B. Lu, C.T.T. Hsu, Stress-strain relations of high-strength concrete, *Cem. Concr. Res.* 36 (2006) 1679–1685.
- [37] M. Kinoshita, M.D. Kotsovos, M.N. Pavlovic, Behavior of concrete under passive confinement, *J. Mater. Conc. Struct. Pavements* 502 (1994) 131–142.
- [38] Z.P. Bažant, T. Tsubaki, Total strain theory and path dependence of concrete, *J. Eng. Mech. Div.* 106 (1980) 1151–1173.
- [39] M.D. Kotsovos, S.H. Perry, Behaviour of concrete subjected to passive confinement, *Mater. Struct.* 19 (1986) 259–264.
- [40] J.C. Lim, T. Ozbakkaloglu, Investigation of the influence of the application path of confining pressure: tests on actively confined and FRP confined concretes, *J. Struct. Eng.* 141 (8) (2015) 04014203.
- [41] C.L. Chin, C.K. Ma, A.Z. Awang, J.Y. Tan, C.B. Ong, W. Omar, Confining stress path dependent stress-strain model for pre-tensioned steel confined concrete, *Eng. Struct.* 201 (2019) 109769.
- [42] H.B. Xiong, J.F. Jiang, B.B. Li, Load path dependence of strain and stress for confined concrete, *Mag. Concr. Res.* 68 (12) (2016) 604–618.
- [43] P. Chen, Y.Y. Wang, C.Y. Liu, Confining stress path-dependent analytical model for FRP-confined concrete and concrete-filled steel tube subjected to axial compression, *Compos. Struct.* 201 (2018) 234–247.
- [44] M.H. Lai, Y.W. Liang, Q. Wang, F.M. Ren, M.T. Chen, J.C.M. Ho, A stress-path dependent stress-strain model for FRP-confined concrete, *Eng. Struct.* 203 (2020) 109824.
- [45] M.H. Lai, W. Song, X.L. Ou, M.T. Chen, Q. Wang, J.C.M. Ho, A path dependent stress-strain model for concrete-filled-steel-tube column, *Eng. Struct.* 211 (2020) 110312.
- [46] J.C.M. Ho, X.L. Ou, M.T. Chen, Q. Wang, M.H. Lai, A path dependent constitutive model for CFFT column, *Eng. Struct.* 210 (2020) 110367.
- [47] S.Q. Lin, Y.G. Zhao, Z.H. Lu, Modified confining stress path dependent analytical model for axially loaded circular normal, high and ultra-high strength concrete-filled steel tube stub columns, *Compos. Struct.* 242 (2020) 112192.
- [48] Q.Q. Liang, S. Fragomeni, Nonlinear analysis of circular concrete-filled steel tubular short columns under axial loading, *J. Constr. Steel Res.* 65 (12) (2009) 2186–2196.
- [49] AIJ, Recommendations for Design and Construction of Concrete Filled Steel Tubular Structures, Architectural Institute of Japan, Tokyo, Japan, 2008, (in Japanese).
- [50] X.F. Yan, Y.G. Zhao, S.Q. Lin, Compressive behaviour of circular CFDST short columns with high- and ultrahigh-strength concrete, *Thin-Walled Struct.* (Under Revision).
- [51] J.S. Fan, M.N. Baig, J.G. Nie, Test and analysis on double-skin concrete filled tubular columns, in: Z.Y. Shen, Y.Y. Chen, X.Z. Zhao (Eds.), *Tubular Structures XII - Proceedings of the 12th International Symposium on Tubular Structures, ISTS 2009*, Shanghai, China, 2009, pp. 407–411.
- [52] T. Ekmekyapar, O.H. Alwan, H.G. Hasan, B.A. Shehab, B.J.M. Al-Eliwi, Comparison of classical, double skin and double section CFST stub columns: Experiments and design formulations, *J. Constr. Steel Res.* 155 (2019) 192–204.
- [53] U.M. Sulthana, S.A. Jayachandran, Concrete confinement effect in circular concrete sandwiched double steel tubular stub-columns, *Int. J. Steel Struct.* 20 (2020) 1364–1377.
- [54] W. Li, D. Wang, L.H. Han, Behaviour of grout-filled double skin steel tubes under compression and bending: Experiments, *Thin-Walled Struct.* 116 (2017) 307–319.
- [55] X.L. Zhao, L.W. Tong, X.Y. Wang, CFDST stub columns subjected to large deformation axial loading, *Eng. Struct.* 32 (2010) 692–703.